Received 5 December 2006
Revised 4 June 2007
Accepted 4 June 2007

Boundary element method for thermal flows using *k*-ε turbulence models

Matjaž Ramšak and Leopold Škerget
Faculty of Mechanical Engineering, University of Maribor, Maribor, Slovenia

Abstract

Purpose – This paper aims to develop a multidomain boundary element method (BEM) for modeling 2D complex turbulent thermal flow using low Reynolds two-equation turbulence models.

Design/methodology/approach – The integral boundary domain equations are discretised using mixed boundary elements and a multidomain method also known as a subdomain technique. The resulting system matrix is an overdetermined, sparse block banded and solved using a fast iterative linear least squares solver.

Findings – The simulation of a turbulent flow over a backward step is in excellent agreement with the finite volume method using the same turbulent model. A grid consisting of over 100,000 elements could be solved in the order of a few minutes using a 3.0 Ghz P4 and 1 GB memory indicating good efficiency.

Originality/value – The paper shows, for the first time, that the BEM is applicable to thermal flows using *k*-ε.

Keywords Flow, Turbulence, Simulation, Boundary-elements methods

Paper type Research paper

1. Introduction

The present work represents the continuity of our previous article Ramšak and Škerget (2005), where an isothermal turbulent flow is modelled using the same numerical algorithm. The thermal energy equation is added in the present paper. Practically, all engineering thermal problems are of a turbulent nature. A boundary element method (BEM) is well known for solving a thermal laminar flow but not for a turbulent flow. Besides, our previous-mentioned article one finds very few BEM solutions for a turbulent flow in the open literature. The solution of a relative simple channel flow using an algebraic and one-equation turbulence models is presented in Škerget *et al.* (1990) and Alujevič *et al.* (1991). Authors Wu and Sugavanam (1978) applied BEM only for a flow kinematics while flow kinetics, which is more complicated part in the turbulent flow, was solved using a finite element method and a low-Reynolds two-equation turbulent model. The solution of a simple 2D turbulent Couette flow and a flow past a finite plate was presented. A thermal flow example is not presented in any of mentioned articles.

A two-equation turbulence models are most commonly used in an engineering practice because of the best ratio between a solution quality and computational economy. From the numerical point of view, a turbulence modelling using two-equation turbulence model is more complicated than a laminar flow modelling. Two additional nonlinear equations are added to the basic nonlinear set of equations governing a laminar flow increasing the nonlinearity of the basic set of equations

International Journal of Numerical Methods for Heat & Fluid Flow
Vol. 18 No. 3/4, 2008
pp. 514-532

0961-5539
DOI 10.1108/09615530810853709

across variable turbulent viscosity. In the case of k-ε turbulent model, two additional equations contains extremely nonlinear source functions connecting them together and slowing down the solution convergence. These source functions became singular near the walls where a special treatment is necessary. From this, we can conclude that a good numerical algorithm solving a laminar flow is necessary and serves as a starting point before the one can proceed to a turbulent flow computations.

The requested properties for a laminar flow solver are the:

(1) stability at a higher Reynolds number values;

(2) accuracy;

(3) economy of the solution; and

(4) ability to a solve high-grid density with high-ratio longest/shortest element.

The property (1) is a common problem using BEM. The stability of our BEM numerical algorithm is the main topic in our previous work Ramšak and Škerget (2004), where considerable effort was done to increase the stability at a convection dominated laminar flows. The result was a stable algorithm at the Reynolds number value up to 50,000 in the case of the laminar flow in a driven cavity example, thus far exceeding the largest value of 15,000 computed using BEM by Rek and Škerget (1994).

The accuracy of the BEM, the property (2), is well known quality of BEM (Brebbia *et al.*, 1984; Grigoriev and Dargush, 1999; Škerget *et al.*, 1999; Ramšak and Škerget, 1999). In comparison to the other numerical methods, the accuracy of BEM is more significant at a lower grid density.

All demanded properties will be fulfilled using the following techniques. The property (4) is concerned with the available computer memory. If the solution domain is treated as a single entity, which is the primary advantage of BEM against other domain numerical techniques, the system matrix is full and non-symmetric. For diffusive problems the matrix dimension is of order of the number of boundary elements. For diffusion-convection problems the matrix dimension is significantly increased by the number of domain nodal points. At this stage, only the integrals of fundamental solution are already wasteful of memory at a higher grid density. An elegant solution is applying multidomain BEM, well known also as a subdomain technique (Telles, 1987; Hriberšek and Škerget, 1996).

If the solution domain is divided to the smallest subdomains in the limiting case the obtained system matrix is similar to those obtained using a finite element method, namely a sparse and a diagonal block banded. The indexed matrix storage for nonzero numbers is introduced thus decreasing the necessary memory of order 10,000 times at a moderate grid density (Ramšak and Škerget, 2000). At a higher grid density, the saving is even higher. Using the multidomain approach, the matrix of a fundamental solution integrals are smaller by the same order. Property (3) considering the economy of computation is also fulfilled using the multidomain approach. A sparse system matrix is ideal for a fast iterative methods solving an algebraic system equations (Hriberšek and Škerget, 1996).

The speed-up factor in comparison to a direct solver is approximately 10,000 already at a moderate grid density (Ramšak and Škerget, 2000). Articles by Škerget *et al.* (1999) and Grigoriev and Dargush (1999) also confirm the stability of multidomain model at high-Reynolds number values.

The structure of the paper follows. In Section 2, the governing equations are stated. In Section 3, the numerical algorithm of BEM for solving a general form of a differential parabolic diffusion convective equation is explained. Numerical example is presented in Section 4, to be followed by conclusions.

2. Governing equations

2.1 Stream function vorticity formulation

The stream function vorticity formulation of Navier Stokes equations is very often used for a 2D laminar flow. Let us mention only two most frequently cited papers namely the benchmark solutions of a driven cavity flow by Ghia *et al.* (1982), and the work by Davis (1983) which is well known benchmark solution for a natural convection in a closed cavity. A simplicity, stability and economy of the computation are the quality of the stream vorticity formulation. The main restriction is its limitation only to a 2D flow.

The stream function vorticity formulation and turbulence we have found only in the three papers. In the first paper by authors Cortella *et al.* (2001), the stream vorticity formulation is used for some kind of an algebraic large eddy simulation using a finite element method. The papers by Elkaim *et al.* (1992) and Abib and Jaluria (1993) present the stream vorticity formulation and a two-equation turbulent model using a control volume method. In this paper, the same governing equations are solved as at previous mentioned papers.

In 2Ds, the stream function Ψ equation can be written as the elliptic PDE:

$$\frac{\partial^2 \Psi}{\partial x_i \partial x_i} = -\omega \tag{1}$$

and is also valid for a turbulent flow. The vorticity ω transport equation for a turbulent flow differs only at the turbulent viscosity ν_{T} which is added to the molecular viscosity ν and can be written as the parabolic PDE:

$$\frac{\partial \omega}{\partial t} + \mathbf{v}_j \frac{\partial \omega}{\partial x_j} = \frac{\partial}{\partial x_j}\left((\nu = \nu_{\mathrm{T}} \frac{\partial \omega}{\partial x_j}\right) + S_\omega, \tag{2}$$

where S_w is source function including body forces, such as buoyancy or rotation. The velocity vector $\mathbf{v}_j$ is defined as:

$$\mathbf{v}_j = \left(\frac{\partial \Psi}{\partial y}, -\frac{\partial \Psi}{\partial x}\right). \tag{3}$$

Let us mention, that equation (2) is not derived from first principles. According to Elkaim *et al.* (1992) and others, the exact equation is so complicated as to be impractical for a variable viscosity turbulent flow. Equation (2) will be accepted as a modelling approximation which has and will prove to be very useful in view of the quality of the numerical predictions.

The transport equations for turbulence kinetic energy and energy dissipation are equivalent as at other formulations of Navier-Stokes equations:

$$\frac{\partial k}{\partial t} + \mathbf{v}_j \frac{\partial k}{\partial x_j} = P - \varepsilon - D + \frac{\partial}{\partial x_j}\left(\left(\nu + \frac{\nu_{\mathrm{T}}}{\sigma_k}\right)\frac{\partial k}{\partial x_j}\right) \tag{4}$$

$$\frac{\partial \varepsilon}{\partial t} + \mathbf{v}_j \frac{\partial \varepsilon}{\partial x_j} = C_{\varepsilon 1} f_1 \frac{\varepsilon}{k} P - C_{\varepsilon 2} f_2 \frac{\varepsilon^2}{k} + E + \frac{\partial}{\partial x_j} \left(\left(\nu + \frac{\nu_T}{\sigma_\varepsilon} \right) \frac{\partial \varepsilon}{\partial x_j} \right), \quad (5)$$

where the turbulent viscosity is related to k and ε via:

$$\nu_T = C_\mu f_\mu \frac{k^2}{\varepsilon}. \quad (6)$$

These equations are written as a general low-Reynolds-number model, where the constants and functions are specified according to the turbulence model. The production term P is common for all models. For 2D examples, the production term is computed as:

$$P = \nu_T \left(2 \left(\frac{\partial v_x}{\partial x} \right)^2 + \left(\frac{\partial v_x}{\partial y} + \frac{\partial v_y}{\partial x} \right)^2 + 2 \left(\frac{\partial v_y}{\partial y} \right)^2 \right)$$

In numerical examples, two models will be used.

The first model is Chien (1982) (CH) using:

$$f_\mu = 1.0 - \exp(-0.0115 y^+),$$

$$f_1 = 1, \quad f_2 = 1 - 0.222 \ \exp\left(- \left(\frac{R_T}{6} \right)^2 \right),$$

$$D = 2\nu \frac{k}{y^2}, \quad E = -2\nu \left(\frac{\varepsilon}{y^2} \right) \exp(-0.5 y^+),$$

$$C_{\varepsilon 1} = 1.35, \quad C_{\varepsilon 2} = 1.8, \quad C_\mu = 0.09,$$

$$\sigma_k = 1.0, \quad \sigma_\varepsilon = 1.3.$$

The wall boundary conditions are:

$$k = 0, \quad \varepsilon = 0 \ \text{at} \ y = 0$$

The second model is Fan *et al.* (1993) (FLB) model with the following constants and functions:

$$f_\mu = 0.4 \frac{f_w}{\sqrt{R_T}} + \left(1 - 0.4 \frac{f_w}{\sqrt{R_T}} \right) \left(1 - e^{-R_v/42.63} \right)^3,$$

$$f_1 = 1, \quad f_2 = \left(1 - \frac{0.4}{1.8} e^{-(R_T/6)^2} \right) f_w^2,$$

$$f_w = 1 - \exp\left(- \frac{\sqrt{R_y}}{2.30} + \left(\frac{\sqrt{R_v}}{2.30} - \frac{R_y}{8.89} \right) \left(1 - e^{-R_y/20} \right)^3 \right),$$

$$D = 0, \quad E = 0, \quad C_{\varepsilon 1} = 1.39, \quad C_{\varepsilon 2} = 1.80, \quad C_\mu = 0.09, \quad \sigma_k = 1.0, \quad \sigma_\varepsilon = 1.3.$$

The wall boundary conditions are:

$$k = 0, \quad \frac{\partial \varepsilon}{\partial y} = 0 \text{ at } y = 0.$$

Let us mention that CH model is using a reduced apparent turbulent dissipation, while FLB model is using a true dissipation. The difference between them is the ε boundary condition and damp functions D and E. The criteria numbers are standard:

$$R_{\mathrm{T}} = \frac{k^2}{\nu\varepsilon}, \quad R_y = \frac{y\sqrt{k}}{\nu}, \quad R_\tau = \frac{yv_\tau}{\nu}, \quad v_\tau = \sqrt{\nu|\omega|_{\mathrm{w}}}, \tag{7}$$

where the y is distance to the nearest wall. The wall friction velocity v_τ is computed using the absolute value of the wall vorticity $|\omega|_{\mathrm{w}}$.

2.2 Thermal energy transport equation

Similar to the modelled turbulent vorticity kinetic transport equation (2), the turbulent transport equation for temperature T can be written using the turbulent viscosity hypothesis as follows:

$$\frac{\partial T}{\partial t} + \mathbf{v}_j \frac{\partial T}{\partial x_j} = \frac{\partial}{\partial x_j}\left(\left(\kappa + \frac{\nu_{\mathrm{T}}}{\sigma_{\mathrm{T}}}\right)\frac{\partial T}{\partial x_j}\right) + \frac{S_{\mathrm{T}}}{\varrho c_p}. \tag{8}$$

The effective heat diffusivity is computed as a sum of the molecular diffusivity denoted by κ and turbulent viscosity divided with constant $\sigma_{\mathrm{T}} = 0.9$. Heat sources are included in source term S_{T} divided with mass density ϱ and specific isobaric heat capacity denoted by c_p.

2.3 Boundary conditions

For a turbulent flow, the boundary conditions for the stream function and vorticity remains the same as at laminar flow. The vorticity boundary condition at the wall changes only when the law of the wall is used (Elkaim *et al.*, 1992).

The boundary condition at the walls yields the known stream function value:

$$\Psi = \bar{\Psi} \tag{9}$$

and its derivative in normal direction to the wall:

$$\frac{\partial \Psi}{\partial n} = \overline{v_{\mathrm{t}}} \tag{10}$$

where $\overline{v_{\mathrm{t}}}$ is the known tangential velocity. As it is well known, this provides no direct condition for the wall vorticity. This is the major difficulty associated with the computation of the vorticity on a solid walls and this difficulty becomes even more restricting when computing turbulent flows with k-ε model because of the wall functions usually associated with the wall vorticity.

If numerical techniques like FEM and FDM are used the wall vorticity u_{w} is computed locally from a near wall stream function distribution. In the work of Ghia *et al.* (1982), the second-order accurate formula is used:

$$\omega_{\mathrm{w}} = -\frac{\partial^2 \Psi}{\partial y^2} = -\frac{\Psi_{J+1} - 2\Psi_J + \Psi_{J-1}}{\Delta y^2}$$

generally not satisfying the vorticity solenoidity condition.

In the present BEM numerical algorithm, the wall vorticities ω_Γ are computed implicitly from the stream function transport equation (1), because Ψ and its normal derivatives are both known boundary conditions. Thus, the BEM integral equations are available at the solution domain boundary Γ for the unknown wall vorticities ω_Γ. This is the significant advantage, because the solenoidity is preserved at each iteration. This approach was successful at a laminar flow simulation and causes no problem at the present turbulent flow example.

Regarding the temperature transport equation (8), the boundary conditions are simple of a Diriclet, Neumann or Cauchy type on the boundary of the computational domain. It could also be any their combination. Of course, applying only the Neumann type of boundary condition at a complete boundary will result in an infinite number of solutions, so at least at one point the temperature value must be prescribed.

3. Numerical solution of a general parabolic diffusive convective transport equation

3.1 Differential form

The differential transport equations for the stream function, vorticity, turbulent kinetic energy, dissipation and temperature can be written in a general form as:

$$\begin{aligned} \frac{Du}{Dl} &= \frac{\partial u}{\partial l} + \mathbf{v}_j \frac{\partial u}{\partial x_j} \\ &= \frac{\partial}{\partial x_j}\, a(x_j, u) \frac{\partial u}{\partial x_j} + S(x_j, u), \end{aligned} \tag{11}$$

where u is an arbitrary scalar field function, $a(x_j,u)$ is a variable diffusivity and $S(x_j,u)$ is a source term. Generally, the variables a and S are nonlinear and in a function of time, place and other field variables.

The finite difference approximation of the field function time derivative at time level l is written as:

$$\frac{\partial u}{\partial t} \approx \frac{u^l - u^{l-1}}{\Delta t},$$

where $\Delta t = t^l - t^{l-1}$ is the time increment. The contribution of the previous time step is added to the source term S as:

$$-\frac{u^{l-1}}{\Delta t}.$$

The fundamental solutions necessary for boundary integral equation are known only for linear differential equations with constant coefficients. The variable diffusivity a is split on constant a and variable part a as:

$$a(x_j, u) = \bar{a} + \bar{a}(x_j, u).$$

Introducing this equation into diffusivity term, the next equivalence is obtained:

$$\frac{\partial}{\partial x_j}\left(a\frac{\partial u}{\partial x_j}\right) = \bar{a}\frac{\partial^2 u}{\partial x_j^2} + \frac{\partial}{\partial x_j}\left(\tilde{a}\frac{\partial u}{\partial x_j}\right).$$

Now, more possibilities are available (Ramšak and Škerget, 2005). The simplest is dealing the second term on the right-hand side as the source term S:

$$S = \frac{\partial}{\partial x_j}\left(\bar{a}(x_j, u)\frac{\partial u^{k-1}}{\partial x_j}\right), \tag{12}$$

where k is the inner iteration index. Similar to the source term treatment, a semi-implicit approach based on the backward Euler scheme as the linearization technique for the convective term is applied. This allows in the case of a vorticity transport equation the direct computation of an intermediate vorticity field based on the known velocity field, computed from the known stream function distribution.

The final differential representation of the parabolic diffusion-convective equation is therefore:

$$\bar{a}\frac{\partial^2 u^l}{\partial x_j^2} - \frac{u^l}{\Delta t} - \mathbf{v}_j^{k-1}\frac{\partial u^l}{\partial x_j} + S^{k-1} = 0, \tag{13}$$

where k is the inner iteration index. For the sake of clarity, the superscript l and k will be omitted in further text.

Boundary conditions on the boundary Γ and the initial conditions in the domain Ω must be known:

$$u = \bar{u}, \quad \text{on } \Gamma_1 \quad \text{for } t \geq t_o \tag{14}$$

$$\frac{\partial u}{\partial n} = \overline{\frac{\partial u}{\partial n}} \quad \text{on } \Gamma_2 \quad \text{for } t \geq t_o, \tag{15}$$

$$u = \bar{u}_o \quad \text{in } \Omega \quad \text{for } t = t_o. \tag{16}$$

When dealing a BEM and a variable diffusivity problem, such as a turbulent flow, the multidomain technique must be applied in order to apply different constant diffusivity at an each subdomain. The second reason for applying the multidomain technique is to make a system and integral matrices sparse, as mentioned in the introduction.

As each subdomain is treated as a single entity, the interface nodes have to communicate results between subdomains. This is possible in an iterative way or much better in an implicit way, where at the interface boundaries between the subdomains I and II the compatibility interface condition for u is applied:

$$u|_{\mathrm{I}} = u|_{\mathrm{II}}, \tag{17}$$

as well as the equilibrium interface condition:

$$\lambda\frac{\partial u}{\partial n}|_{\mathrm{I}} = -\lambda\frac{\partial u}{\partial n}|_{\mathrm{II}}, \tag{18}$$

where λ is a diffusion factor for the sake of generality. For example, $\lambda = \nu + (\nu_T/\sigma k)$ when dealing turbulent kinetic energy transport equation.

3.2 Integral form

The general form of the differential parabolic diffusion-convective equation (13) can be transformed into an equivalent integral statement (Brebbia *et al.*, 1984; Škerget *et al.*, 1999):

$$0 = -c(\xi)u(\xi) - \bar{a}\int_\Gamma u\frac{\partial u^*}{\partial n}\mathrm{d}\Gamma + \bar{a}\int_\Gamma \frac{\partial u}{\partial n}u^*\mathrm{d}\Gamma \quad \text{diffusion} - \int_\Gamma u\mathbf{v}_j\mathbf{n}_j u^*\mathrm{d}\Gamma + \int_\Omega u\mathbf{v}_j\frac{\partial u^*}{\partial x_j}\mathrm{d}\Omega, \quad \text{convection} + \int_\Omega Su^*\mathrm{d}\Omega, \quad \text{source } S \tag{19}$$

where $\mathbf{n}_j$ is the unit normal vector to the boundary element at the nodal point. The variable u^* is modified Helmholtz fundamental solution (Ramšak and Škerget, 2005). Other fundamental solutions can be applied, e.g. an elliptic diffusion-convective (Škerget *et al.*, 1999), but we have used the modified Helmholtz fundamental solution in presented numerical example.

3.3 Discrete form

Let us introduce some notation comments. The integral equation (19) is valid for any arbitrary geometry. From now on, in order to distinguish the solution domain Ω and its exterior boundary Γ from the subdomain geometry, the subdomain domain is denoted by Ω_s and the subdomain boundary by Γ_s consistently. The subscript e is used to denote a boundary element.

Following the mixed boundary elements idea, the simplest possible discretisation is the continuous linear field function approximation over the boundary element and the constant approximation of its derivative in the normal direction to the boundary element (normal flux) (Figure 1). The main reason for this is to keep the numerical scheme as simple as possible. Regarding the storage and CPU cost, we prefer to use a larger number of linear subdomains rather than a smaller number of higher order subdomains. Another reason is that the higher order elements are more sensible to stability problems than lower order ones.

An unknown field function u is approximated with a continuous linear interpolation polynomials over the boundary element $\Phi^{n=2}$ (Figure 1(a)):

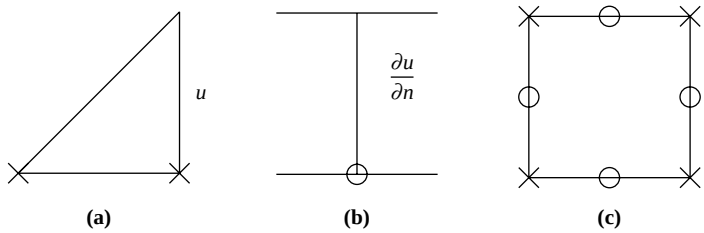

Notes: The × denotes a function u boundary nodes and the o denotes a normal flux $\partial u/\partial n$ boundary nodes

Figure 1. Continuous linear approximation over a boundary element $n = 2$ (figure a) and subdomain approximation $N = 4$ (figure c). Discontinuous constant normal flux approximation over boundary element $(n = 1)$ (figure b)

$$\Phi^{n=2} = \frac{1}{2}\begin{Bmatrix} 1-\xi \\ 1+\xi \end{Bmatrix}, \tag{20}$$

where $\xi \in [-1,1]$ is the local coordinate system and $n = 2$ is the degree of freedom. The unknown normal flux is approximated with constant interpolation polynomials $\Phi^{n=1}$ as:

$$\Phi^{n=1} = \{1\}, \tag{21}$$

Next, the function domain approximation has to be dealt with. The subdomain is surrounded by four boundary elements (Figure 1(c)). The two neighbouring boundary elements share the same function boundary nodal point, i.e. the subdomain vertex, with only one unknown or known value. When using different nodal points for the function approximation over the boundary elements and the domain, for example, in the case of the discontinuous approximation (Škerget *et al.*, 1999), the discretisation of the boundary and the domain integrals, resulting from the convective term, leads to additional numerical error due to transformations between nodal points, which can present a source of numerical instabilities in convection dominated flows. Thus, the same interpolation nodal points for boundary and domain approximation are preferable in a BEM discretisation, and this is one of the major advantages of the mixed element discretisation approach. In this case, the function domain interpolation φ^N is trivial bilinear using $N = 4$ boundary nodal points and given by:

$$\phi^{N=4} = \frac{1}{4}\begin{Bmatrix} 1-\xi-\eta+\xi\eta \\ 1+\xi-\eta-\xi\eta \\ 1+\xi+\eta+\xi\eta \\ 1-\xi+\eta-\xi\eta \end{Bmatrix}, \tag{22}$$

where $\xi,\eta \in [-1,1]$ are again local coordinate system. It should be mentioned that variable diffusivity a and source function S are approximated with the same domain functions as u, equations (22).

With the interpolation polynomials defined, the boundary integrals of the fundamental solution u^* over the individual boundary element Γ_e are written as:

$$h^n = \int_{\Gamma_e} \Phi^n \frac{\partial u^*}{\partial n} \mathrm{d}\Gamma_e, \quad g^n = \int_{\Gamma_e} \Phi^n u^* \mathrm{d}\Gamma_e, \tag{23}$$

and the domain integrals over individual subdomain Ω_s are:

$$d_j^N = \int_{\Omega_s} \phi^N \frac{\partial u^*}{\partial x_j} \mathrm{d}\Omega_s, \quad d^N = \int_{\Omega_s} \phi^N u^* \mathrm{d}\Omega_s. \tag{24}$$

The integrals are functions of the geometry and material properties. In the case of the Helmholtz fundamental solution, the remaining variable is a diffusivity. In the case of a laminar flow computation, the integrals have to be computed only once at the beginning of the computation. When computing a turbulent flow, turbulent viscosity

changes each iteration and one should keep in mind that integrals should be recomputed each iteration. In this work, two optimisation approaches are used. First, integrals are computed each n iterations since the turbulent viscosity changes only a little each iteration. Usually, this value is ten iterations and higher values. The principle of second optimisation procedure is that only the integrals where the average cell turbulent viscosity changes more than p-per cent are computed. The usually value of p is approx. 1 per cent and this value has a minimal influence on results. With this optimisation, the necessary CPU for integration is of order few percent to the overall CPU. A Gaussian quadrature rule is used to evaluate integrals of a fundamental solution. Details on the numerical integration are given in Rek and Škerget (1994).

The complete boundary integral equation over the subdomain boundary Γ_s will be written as the sum of all individual boundary integrals Γ_e surrounding the subdomain. In the vertex nodal point the contribution $\{h\}$ of both neighbouring boundary integrals Γ_e could be summed up as $\{h\prime\}$. The obtained boundary integral over the subdomain boundary Γ_s has $N = 4 \times (n - 1) = 4$ degrees of freedom. The boundary integral discretisation has the following form:

$$\begin{aligned} \int_{\Gamma_s} \frac{\partial u^*}{\partial n}\, u \mathrm{d}\Gamma_s &= \sum_{e=1}^{4} \left\{ \int_{\Gamma_e} \Phi^n \frac{\partial u^*}{\partial n} \mathrm{d}\Gamma_e \right\}^{\mathrm{T}} \\ \{u\}^n &= \sum_{e=1}^{4} \{h^n\}^{\mathrm{T}} \\ \{u\}^n &= \sum_{i=1}^{N=4} \{h'\}^{\mathrm{T}} \{u\}^N, \end{aligned} \tag{25}$$

where the last sum represents the loop over $N = 4$ interpolation boundary nodal points. The boundary integrals $\{\mathrm{h}'\}$ and domain integrals $\{d_j\}$ and $\{d\}$ over the subdomain (equation 24) share the same nodal points and could be added together at each nodal point.

The normal flux interpolation is simple. As mentioned before, the constant approximation of the normal flux is prescribed to the boundary element, equation (21). The boundary integral of the normal flux over the complete boundary of subdomain Γ_s is computed as a sum of four individual boundary integrals Γ_e. Thus, the four elements with only one nodal point each, are written as:

$$\begin{aligned} \int_{\Gamma_s} \frac{\partial u}{\partial n}\, u^* \mathrm{d}\Gamma_s &= \sum_{e=1}^{4} \left\{ \int_{\Gamma_e} \Phi^n u^* \mathrm{d}\Gamma_e \right\}^{\mathrm{T}} \\ \left\{ \frac{\partial u}{\partial n} \right\}^n &= \sum_{e=1}^{4} \{g^n\}^{\mathrm{T}} \\ \left\{ \frac{\partial u}{\partial n} \right\}^n &= \sum_{i=1}^{M=4} \{g\}^{\mathrm{T}} \left\{ \frac{\partial u}{\partial n} \right\}^M, \end{aligned} \tag{26}$$

where the last sum represents the loop over all $M = 4$ boundary normal flux nodal points. The boundary integral equation (19) are written for an individual subdomain

in discrete form using discrete equations for function (25) and the normal flux equation (26):

$$0 = -c(\xi)u(\xi) - \bar{a}\sum_{i=1}^{N}\{h'\}^{\mathrm{T}}\{u\}^{N} + \bar{a}\sum_{i=1}^{M}\{g\}^{\mathrm{T}}\left\{\frac{\partial u}{\partial n}\right\}^{M} - \sum_{i=1}^{N}\{g_j\}^{\mathrm{T}}\{uv_j\}^{N} + \sum_{i=1}^{N}\{d_j\}^{\mathrm{T}}\{uv_j\}^{N} + \sum_{i=1}^{N}\{d\}^{\mathrm{T}}\{S\}^{N}, \tag{27}$$

where index i means the sum over $N = 4$ function nodal points and $M = 4$ normal flux nodal points of individual subdomain (Figure 1). The terms containing (un)known function u could be added together as:

$$0 = \sum_{i=1}^{N}\{ -(c(\xi) + \bar{a}h') + (-g_j + d_j)v_j\}^{\mathrm{T}}\{u\}^{N} + \bar{a}\sum_{i=1}^{M}\{g\}^{\mathrm{T}}\left\{\frac{\partial u}{\partial n}\right\}^{M} + \sum_{i=1}^{N}\{d\}^{\mathrm{T}}\{S\}^{N}.$$

The new variable e is introduced as:

$$e = -(c(\xi) + \bar{a}h') + (-g_j + d_j)v_j$$

and scalar f of a known value:

$$f = \sum_{i=1}^{N}\{d\}^{\mathrm{T}}\{S\}^{N}.$$

Using new variables, the discretised integral equation for the subdomain is written as:

$$\sum_{i=1}^{N}\{e\}^{\mathrm{T}}\{u\}^{N} - \sum_{i=1}^{M}\{g\}^{\mathrm{T}}\left\{\frac{\partial u}{\partial n}\right\}^{M} = f. \tag{28}$$

The equation (28) is the discrete form of the integral boundary equation (19) at the source point ξ. The complete system matrix for one subdomain is obtained by writing the equation (28) for all function and normal flux subdomain nodal points. The source point is thus located in $\xi = 1, N$ function nodal points and $\xi = 1, M$ normal flux nodal points resulting in eight equations written as:

$$[E]\{u\} - [G]\left\{\frac{\partial u}{\partial n}\right\} = \{f\}. \tag{29}$$

3.3.1 Implementation of boundary conditions on boundaries of computational domain. The nodal points on boundaries of computational domain are described first, as they are dependent on the physical conditions, relating computational domain to its surroundings. On the contrary, the interface conditions, which have to be imposed between the subdomains, are formally the same for all nodal points on subdomain interface boundaries.

The matrix form of discrete boundary integral equation (29) is transformed to the system of algebraic equations by applying the boundary condition (14), the known

function value $\bar{u}$ on the boundary Γ_1 and the known normal flux value $\overline{\partial u/\partial n}$ on Γ_2 equation (15):

$$\begin{bmatrix} [-G]^{\Gamma_1} \\ [E]^{\Gamma_2} \end{bmatrix} \cdot \begin{Bmatrix} \left\{\frac{\partial u}{\partial n}\right\}\Gamma_1 \\ \{u\}\Gamma_2 \end{Bmatrix} = \begin{Bmatrix} -[E]\{\bar{u}\}\Gamma_1 \\ [G]\left\{\overline{\frac{\partial u}{\partial n}}\right\}\Gamma_2 \end{Bmatrix} + \{f\},$$

which can be further written as:

$$[A]\{x\} = \{B\}. \tag{30}$$

3.3.2 Implementation of interface conditions between subdomains. The normal flux and function nodal points on the boundary element are treated differently, due to the different interpolation nodes connectivity. We will consider them separately (Figure 2).

3.3.3 Normal flux boundary element nodal points. Two flux points in contact on the interface between two subdomains I and II are considered as shown on the left-hand side (Figure 2). In subdomain I, the unknown flux value at nodal point I is denoted as $\partial u/\partial n_{\mathrm{I}}$. Following the same notation, $\partial u/\partial n_{\mathrm{II}}$ is the unknown value in subdomain II. The discretised integral boundary equation (28) can be written for subdomain I as:

$$\left(\sum_{i=1}^{N} \{e\}^{\mathrm{T}}\{u\}^{N}\right)_{\mathrm{I}} - \left(\sum_{i=1}^{M-1} \{g\}^{\mathrm{T}}\left\{\frac{\partial u}{\partial n}\right\}^{M-1} + g_{\mathrm{I}}\frac{\partial u}{\partial n_{\mathrm{I}}}\right)_{\mathrm{I}} = f_{\mathrm{I}}$$

and for the subdomain II as:

$$\left(\sum_{i=1}^{N} \{e\}^{\mathrm{T}}\{u\}^{N}\right)_{\mathrm{II}} - \left(\sum_{i=1}^{M-1} \{g\}^{\mathrm{T}}\left\{\frac{\partial u}{\partial n}\right\}^{M-1} + g_{\mathrm{II}}\frac{\partial u}{\partial n_{\mathrm{II}}}\right)_{\mathrm{II}} = f_{\mathrm{II}}$$

where the integrals with index I are computed for subdomain I and the integrals II for subdomain II. For the sake of simplicity, the sum terms on the left side of equations will be omitted in the further text. From the equilibrium interface condition (18), an additional equation is obtained which reduces the number of unknowns from two to one. The value of $\partial u/\partial n_{\mathrm{I}}$ at subdomain I is chosen to be the unknown flux. This decision could be done for the second unknown variable and is arbitrary. With this unknown chosen, the above equations can be rewritten as:

$$-g_{\mathrm{I}}\frac{\partial u}{\partial n_{\mathrm{I}}} = f_{\mathrm{I}},$$

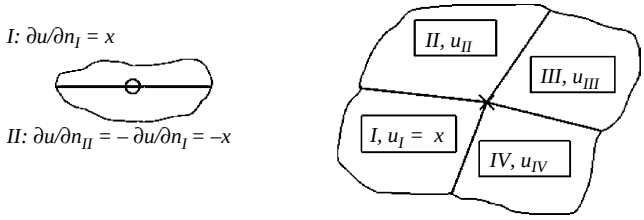

Figure 2.
The normal flux (left) and the function (right) nodal points on the boundary element and implementation of the interface boundary condition

Notes: A subdomain indexes are I, II, III and IV

$$+\frac{\lambda_{\mathrm{I}}}{\lambda_{\mathrm{II}}} g_{\mathrm{II}} \frac{\partial u}{\partial n_{\mathrm{I}}} = f_{\mathrm{II}},$$

to form an over-determined system of two equations with only one unknown.

3.3.4 Function boundary element nodal points. Because of topological aspects of the vertex points, see Figure 2 (right), the application of the interface boundary conditions to the subdomain vertex nodal points are not so straightforward as for the flux points.

The discrete form of the integral boundary equation (28) is written for subdomain I at the vertex nodal point I as:

$$e_{\mathrm{I}} u_{\mathrm{I}} = f_{\mathrm{I}}$$

where the rest sums are omitted again. In a similar way, the other three equations are obtained at subdomains II-IV:

$$e_{\mathrm{II}} u_{\mathrm{II}} = f_{\mathrm{II}}$$

$$e_{\mathrm{III}} u_{\mathrm{III}} = f_{\mathrm{III}}$$

$$e_{\mathrm{IV}} u_{\mathrm{IV}} = f_{\mathrm{IV}}$$

forming together four linear independent equations. The implementation of the function compatibility interface condition is straightforward. Similar as before at the flux nodal points, the u_{I} is chosen to be unknown function value at the vertex nodal point. The compatibility interface condition is rewritten as:

$$u_{\mathrm{I}} = u_{\mathrm{II}} = u_{\mathrm{III}} = u_{\mathrm{IV}}.$$

To summarise, four equations are available with only one unknown, leading to the over-determined system matrix.

3.4 Solving the over-determined system of equations

The over-determined system matrix $\mathbf{A}$ is sparse and block structured. The iterative linear least squares solver of Paige and Saunders (1982) is used to obtain the solution to the system of equations. It is analytically equivalent to the standard method of conjugate gradients, (for details see Paige and Saunders, 1982). To accelerate the convergence, a diagonal preconditioning method is applied (Ramšak and Škerget, 2000).

4. Turbulent flow over a backward-facing step

Turbulent flow over a backward-facing step is one of the most popular tests for turbulence models and numerical methods, as well as for studies of the physics of separating and reattaching turbulent flows. The problem definition, geometry and boundary conditions are the same as in the work by Hanjalić and Jakirlić (1998) (Figure 3). They have used Reynolds stress model (RSM). In addition, the results will be compared to direct numerical simulation (DNS) by Lee *et al.* (1997), CFX 4.0 using Launder-Sharma near wall turbulent model, FVM and CH model by Bredberg (2001) and the experimental data by Jović and Driver (1994). The most crucial comparison will be with FVM both using the same turbulent model.

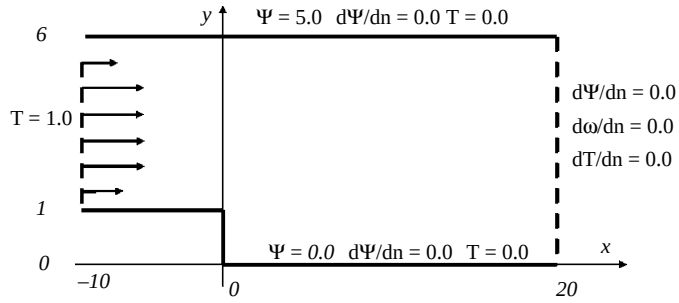

Note: Geometry and boundary conditions

Figure 3.
Turbulent flow over a backward-facing step

The developed numerical algorithm for solving a general transport equation is verified using a nonlinear diffusion and a turbulent channel flow example in our previous work Ramšak and Škerget (2005). The results show good accuracy.

The Reynolds number is based on the average inlet velocity and the step height H. Its value is $Re_H = 5{,}000$. The inlet height is $5H$ giving expansion ratio 1.2. The solution domain covers $10H$ prior to the step and $20H$ downstream from the step (Figure 3). This size of domain was adopted to coincide with that used for the DNS and RSM in mentioned articles.

The boundary conditions are equivalent to those in the work by Hanjalić and Jakirlić (1998) (Figure 3). The inlet profiles of velocity, turbulent kinetic energy and dissipation are obtained using the preliminary channel flow computation. The channel width is $5H$ and the viscosity value is the same as at backward-facing step flow simulation giving the Reynolds number value of $Re_{5H} = 25,000$ (Figure 4).

The coarsest grid A has 8,500 elements, while the finest has 76,500 elements. The post-step domain at grid A has 100×50 elements clustered in the regions close to the walls and in the shear layer (Figure 5). In comparison, the RSM results by Hanjalić are obtained using comparable grid of 90×46 control volumes in post-step domain. Our second grid B had 200×120 and the finest grid C had 300×180 elements in that region. The first point near the wall was at $y+ \approx 10{,}5{,}2$ for A,B,C grid, respectively, at outlet region. At the recirculation region, the $y+$ values are much lower.

The steady turbulent solutions are computed using very large time step value of $\Delta t = 10^{16}$. The results of laminar flow computation at $Re_H = 100$ are used as the initial solution for stream function and vorticity. The stream function under relaxation factor is URF$\psi = 1.0$. All other under relaxation values are 0.01. The convergence criteria is 10^{-4} for all computations.

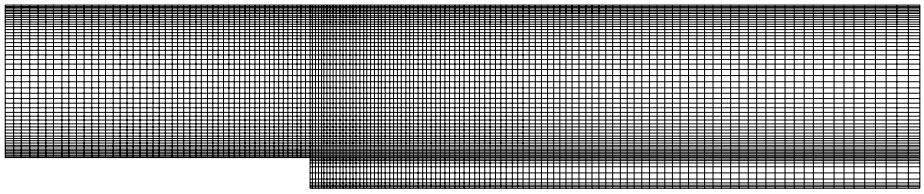

Note: The coarsest grid using 8,500 elements

Figure 4.
Turbulent flow over a backward-facing step

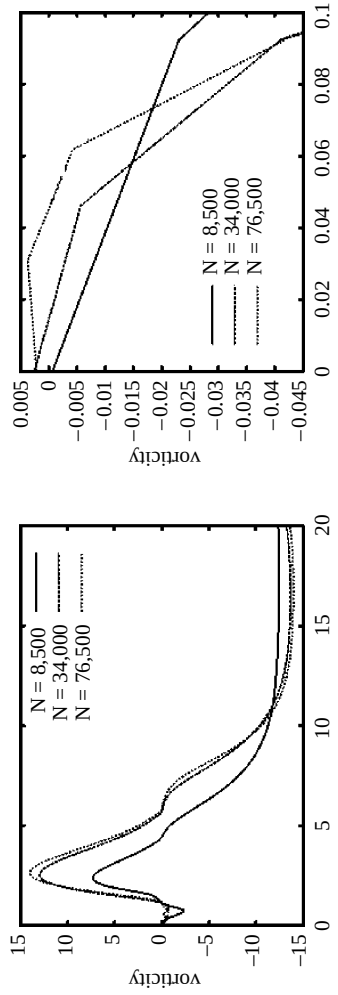

Notes: The vorticity profiles at a lower wall and a different grid density using BEM and CH turbulence model. The existence of the corner bubble is evident by vorticity changing the sign at grids using N = 34,000 and 76,500, see right hand side figure where the corner area of left hand side figure is enlarged

Figure 5.
Turbulent flow over a backward-facing step

We discuss now the computational results shown in Table I as a comparison of reattachment lengths. First the grid refinement or nodalization analysis is discussed. Convergence of reattachment lengths to the specific value is evident for BEM using CH model. Next, the reference solution must be selected. According to the basic fluid mechanics rules, the experiment is the one to compare to. In the other hand, it is well known that the comparison of 2D numerical simulation with experiment, which is always 3D, is questionable. Eliminating the experiment as the reference solution the situation is clear. The DNS results by Lee *et al.* (1997) is the reference solution for our simulations. As expected, the RSM reattachment length is the closest to DNS solution, both agreeing well to the experiment (Table I). Surprisingly, the RSM reattachment length is over predicting, while k-ε models results are all under predicting.

Keeping in mind that the main aim of this example is to validate the BEM numerical scheme for complex turbulent flows, the most crucial comparison is using the same turbulent model and a different numerical algorithm. In this case, the excellent agreement of re-attachment point less than 1 per cent is obtained between the BEM 5.81 and the FVM 5.86 by Bredberg (2001) both using CH model. The computations by Bredberg were made using the finite-volume method code CALF-BFC. The SIMPLE-C algorithm is used to deal with the velocity-pressure coupling in contrast to the stream function – vorticity formulation used in this paper.

The comparison between the k-ε results computed in this work follows. Far the best results are obtained using BEM and CH model, following CFX (CFX 5.5, 2001) and LS model and the last is BEM and FLB model (Figure 6). From Figure 5, where the vorticity profiles at lower wall are shown, the corner bubble is clearly seen using higher grid density B and C. As suspected, the influence of the turbulent model used is much higher than the numerical method used. Velocity profile prior to reattachment point of the mean vortex are shown in Figure 7 showing good agreement between both BEM computations and the CFX result.

In Figure 8, the temperature contour lines are shown in the recirculation zone. The reattachment points are more clearly indicated with the local Nusselt number fall in the Nusselt plot at the lower wall (Figure 9). Comparing with the Nusselt number profile at upper wall, the recirculation zone significantly decreases the heat flux rate.

Recirculation	Mean	Secondary	Third
CFX LS $N = 8{,}500$	4.61	0.36	–
CFX LS $N = 34{,}000$	5.27	0.97	
BEM FLB $N = 8{,}500$	3.07	0.16	–
BEM FLB $N = 34{,}000$	4.52	0.30	
BEM CH $N = 8{,}500$	4.28	1.21	–
BEM CH $N = 34{,}000$	5.72	1.14	0.014
BEM CH $N = 76{,}500$	5.81	1.19	0.045
CH (Bredberg, 2001)	5.86	?	?
RSM (Hanjalić and Jakirlić 1998)	6.38	1.55	0.042
DNS (Lee *et al.*, 1997)	6.28	1.76	0.040
exp (Jović and Driver, 1994)	6.10	?	?

Table I. Turbulent flow over a backward-facing step. Comparison of reattachment lengths

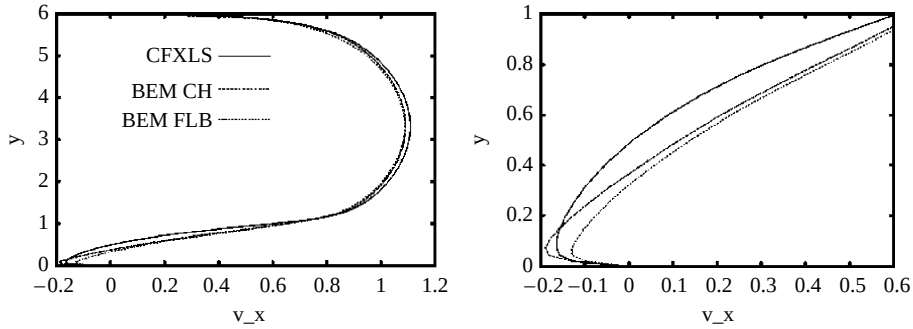

Figure 6.
Turbulent flow over a backward-facing step

Notes: The velocity profile comparison in a recirculation region at x = 3/H. The right hand side figure is enlargement of left hand side figure at bottom area

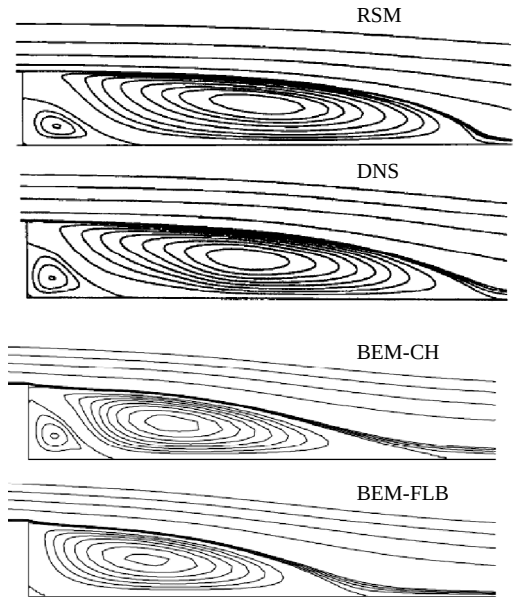

Figure 7.
Turbulent flow over a backward-facing step

Note: Computed streamlines for DNS, RSM and BEM

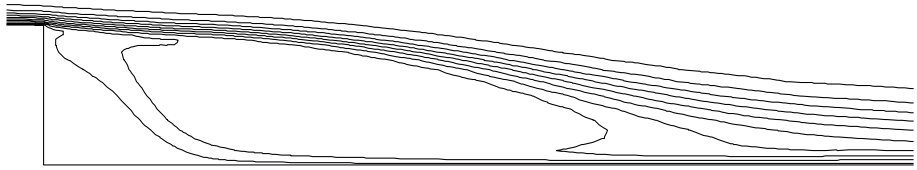

Figure 8.
Turbulent flow over a backward-facing step

Note: Temperature contour plot at a recirculation zone

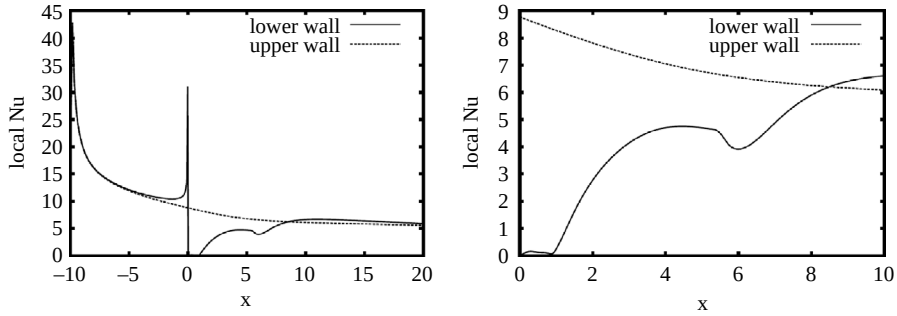

Figure 9.
Turbulent flow over a backward-facing step

Notes: Local Nusselt number profile at walls. On the right hand side of Figure is zoomed recirculation region, where the reattachment points are clearly indicated

5. Conclusions

A BEM has been developed to solve a thermal turbulent flow using the stream function vorticity formulation and low-*Re* k-ε turbulence models. For the first time, a BEM numerical algorithm has been used to solve a complex nonisothermal turbulent flow with a recirculation region.

The turbulent flow over a backward-facing step example shows excellent agreement of less than 1 per cent of the re-attachment point between BEM and FVM code both using the same CH turbulence model (Table I). As expected, the comparison with DNS and RSM computed reattachment lengths are under predicted using k-ε turbulence models.

References

Abib, A.H. and Jaluria, Y. (1993), "Generation of stable thermal stratification by turbulent flows in a partially open closers", *ASME Fundamentals of Natural Convection*, Vol. 264, pp. 127-40.

Alujevič, A., Kuhn, G. and Škerget, L. (1991), "Boundary elements for the solution of Navier-Stokes equations", *Comp. Meth. in App. Mech. and Engin.*, Vol. 91, pp. 1187-201.

Brebbia, C.A., Telles, J.C.F. and Wrobel, L.C. (1984), *Boundary Element Methods, Theory and Applications*, Springer, New York, NY.

Bredberg, J. (2001), "On two-equation eddy-viscosity models", Internal Report 01/8, Chalmers University, Göteborg.

CFX 5.5 (2001), AEA Technology Engineering Software.

Chien, K.Y. (1982), "Predictions of channel and boundary-layer flows with a low-Reynolds-number turbulence model", *AIAA Journal*, Vol. 20, pp. 33-8.

Cortella, C., Manzan, M. and Comini, G. (2001), "CFD simulation of refrigerated display cabinets", *Int. J. of Refrigeration*, Vol. 24, pp. 250-60.

Davis, G.D.V. (1983), "Natural convection of air in a square cavity: a bench mark numerical solution", *Int. J. Num. Meth. Fluids*, Vol. 3, pp. 249-64.

Elkaim, D., Reggio, M. and Camarero, R. (1992), "Simulating a two-dimensional turbulent flow using the k-ε model and the vorticity-stream function formulation", *Int. J. Num. Meth. Fluids*, Vol. 14, pp. 961-80.

Fan, S., Lakshminarayana, B. and Barnett, M. (1993), "Low-Reynolds-Number k-ε model for unsteady turbulent boundary layer flows", *AIAA Journal*, Vol. 31 No. 10, pp. 1777-84.

Ghia, U., Ghia, K.N. and Shin, C.T. (1982), "High-re solutions for incompressible flow using the Navier-Stokes equations and a multigrid method", *J. Com. Phys.*, Vol. 48, pp. 387-411.

Grigoriev, M.M. and Dargush, G.F. (1999), "A poly-region boundary element method for incompressible viscous fluid flows", *Int. J. Num. Meth. Fluids*, Vol. 46, pp. 1127-58.

Hanjalić, K. and Jakirlić, S. (1998), "Contribution towards the second-moment closure modelling of separating turbulent flows", *Computers & Fluids*, Vol. 27, pp. 137-56.

Hriberšek, M. and Škerget, L. (1996), "Iterative methods in solving Navier-Stokes equations by the boundary element method", *Int. Jour. Numer. Meth. Fluids*, Vol. 39, pp. 115-39.

Jović, S. and Driver, D.M. (1994), "Backward-facing step measurements at low Reynolds number $Re_H = 5000$", TM 108807, NASA.

Lee, H., Moin, P. and Kim, J. (1997), "Direct numerical simulation of turbulent flow over a backward-facing step", *J. Fluid Mech.*, Vol. 330, p. 349.

Paige, C.C. and Saunders, M.A. (1982), "LSQR: sparse linear equations and least-squares problems", *ACM Transactions on Mathematical Software*, Vol. 2, pp. 195-209.

Ramšak, M. and Škerget, L. (1999), "Mixed boundary elements for laminar flows", *Int. Jour. Numer. Meth. Fluids*, Vol. 31, pp. 861-77.

Ramšak, M. and Škerget, L. (2000), "Iterative least squares methods for solving over-determined matrix for mixed boundary elements", *ZAMM, Berlin*, Vol. 80, Supplement 3, pp. 657-8.

Ramšak, M. and Škerget, L. (2004), "A subdomain boundary element method for high-Reynolds laminar flow using stream function-vorticity formulation", *Int. Jour. Numer. Meth. Fluids*, Vol. 46, pp. 815-47.

Ramšak, M. and Škerget, L. (2005), "A multidomain boundary element method for two equation turbulence model", *Eng. Analysis with Boundary Elements*, Vol. 29, pp. 1086-103.

Rek, Z. and Škerget, L. (1994), "Boundary element method for steady 2D high-Reynolds number flow", *Int. Jour. Numer. Meth. Fluids*, Vol. 19, pp. 343-61.

Škerget, L., Hriberšek, M. and Kuhn, G. (1999), "Computational fluid dynamics by boundary-domain integral method", *Int. Jour. Numer. Meth. Fluids*, Vol. 46, pp. 1291-311.

Škerget, L., Alujevič, A., Zagar, I. and Rek, Z. (1990), "Boundary element method for laminar and turbulent flow of incompressible viscous fluid", *YU Term 90 Proceedings*, pp. 35-50.

Telles, J.C. (1987), "A self adaptive coordinate transformation for efficient numerical evaluation of general boundary element integrals", *Int. J. Num. Meth. Eng.*, Vol. 24, pp. 959-73.

Wu, J.C. and Sugavanam, A. (1978), "Method for the numerical solution of turbulent flow problems", *AIAA*, Vol. 16, pp. 948-55.

Corresponding author
Matjaž Ramšak can be contacted at: matjaz.ramsak@uni-mb.si